Journal of
RAMAN SPECTROSCOPY WILEY

The Raman Laser Spectrometer: A performance study using ExoMars representative crushed samples

Carlos Perez Canora[1] | Jose Antonio Rodriguez[2] | Fabio Musso[3] |
Andoni Moral[1] | Laura Seoane[1] | Jesus Zafra[1] |
Pablo Rodriguez Rodriguez[1] | Sergio Ibarmia[1] | Marina Benito[1] |
Marco Veneranda[4] | Jose Antonio Manrique[4] | Gonzalo Ramos[1] |
Elena Charro[4] | Jose Manuel Lopez[4] | Manuel Ángel González[4] |
Ian Hutchinson[5] | Olga Prieto-Ballesteros[6] | Fernando Rull[4] |
Guillermo Lopez-Reyes[4]

[1]Space Deparment, Instituto Nacional de Técnica Aeroespacial (INTA), Torrejón de Ardoz, Spain

[2]Ingeniería de Sistemas para la Defensa de España S. A., Madrid, Spain

[3]Thales Alenia Space Italy, Turin, Italy

[4]Condensed Matter Physics, Crystallography and Mineralogy, Universidad de Valladolid, Valladolid, Spain

[5]Department of Physics and Astronomy, University of Leicester, Leicester, UK

[6]Department of Planetology and Habitability, Centro de Astrobiología (CSIC-INTA), Madrid, Spain

Correspondence
Carlos Perez Canora, Space Deparment, Instituto Nacional de Técnica Aeroespacial (INTA), Ctra. Ajalvir km. 4, 28850 Torrejón de Ardoz, Spain.
Email: carlos.perez@cab.inta-csic.es

Abstract

The Raman Laser Spectrometer (RLS) is one of three key analytical instruments incorporated within the body of the ExoMars 2022 rover. The rover will collect samples from different sites on the Oxia Planum plain, using a drill capable of penetrating the near subsurface and rocky outcrops to a depth of 2 m. Samples are passed to the Analytical Laboratory Drawer (ALD) in the heart of the rover vehicle, where the Sample Preparation and Distribution System (SPDS) processes and transports the crushed material into a refillable container (RC), which is then presented to the analytical instruments for exobiology and geological investigation. The final sample grain distribution of the powder sample following the crushing and flattening processes is a critical aspect of the RLS instrument that has a direct impact on its overall performance, related to its mineral identification and operational capabilities. This paper provides a comparative overview of the performance of a set of Raman instruments, the RLS micro-Raman Laboratory Equipment, the RLS ExoMars Simulator, and the RLS Engineering and Qualification Model (EQM) using Martian representative crushed samples, along with an evaluation of instrument performance as a function of the operational scenario. The results from the work performed by the RLS team confirm the capability of the RLS instrument performances, by acquiring good-quality spectra from crushed samples provided by the SPDS, whose science return can be further optimized when improving the RLS instrument operation sequence.

KEYWORDS

crushed samples, ExoMars, operational scenario, Raman, RLS

1 | INTRODUCTION

The ExoMars program[1] aims to investigate the Martian environment and mature new technologies in order to pave the way for a future Mars sample return mission. To achieve these objectives, the Rosalind Franklin ExoMars rover will collect scientific samples from different locations on the Martian surface, using the rover's drill capable of penetrating well into the subsurface and rocky outcrops (2 m). The drill represents a key element for the scientific success of ExoMars because it will provide access to potentially well-preserved organic molecules.

The samples extracted by the drill (a core of roughly 3 cm length by 1 cm diameter or a collection of fragments and powder) are passed to the Analytical Laboratory Drawer (ALD)[1] in the heart of the rover vehicle, where the Sample Preparation and Distribution System (SPDS),[1] which is composed of several mechanisms, processes and prepares the sample for dedicated exobiology and geological research. Samples are dropped into the SPDS crushing station (CS) to produce a powder with the desired particle size distribution. This powder is further distributed by a dosing mechanism, which fills the sample refillable container (RC) where the sample material is finally flattened and then presented to each of the analytical instruments in turn (i.e., the Raman Laser Spectroscopy instrument [RLS],[2] the visual plus IR spectroscopy instrument [MicrOmega],[3,4] and the laser desorption mass spectrometry [MOMA-LDMS],[5] which are designed to perform detailed chemical, physical, and spectral analyses, respectively).

As a key part of the Pasteur payload (PPL) inside the ExoMars Rover,[1] RLS is a powerful tool for the structural and compositional analysis of samples. The RLS instrument, which was developed by an international consortium led by Spain (i.e., France, United Kingdom, and Germany), was designed around a modular concept, in which three separate units are connected by the means of electrical and optical harnesses.[2] The Instrument Control and Excitation Unit (ICEU) provides the laser excitation (532 nm)[6] signal and performs the overall operational control of the instrument. The Spectrometer Unit (SPU)[7] performs the spectral acquisition. A Charge-Coupled Device (CCD) images the light produced by a grating and transfers the data obtained to the ICEU. The internal optical head (iOH)[8] focuses the excitation laser light onto the surface of the crushed sample, maximizing the signal-to-noise ratio (SNR) obtained, and collects the Raman light produced by the sample (an optical fiber then directs this light to the SPU). The RLS instrument also utilizes two dedicated RLS calibration targets (CTs). These disks are manufactured from polyethylene terephthalate that produces Raman bands

across the RLS spectral range and so can be used for calibration and verification of the instrument throughout the mission.[9] The interfaces between the RLS[2] instrument and the ALD were defined specifically for each RLS unit, given each set of particular requirements. Substantial significant effort was invested in order to characterize and verify the performance of the RLS iOH as it implements the critical and dedicated interface to the sample (i.e., ensure that the optimum focusing distance is achieved). The RLS iOH, located above the sample distribution mechanism (SPDS), allows direct sample observation through an optical window, which prevents contamination from the iOH to the sample area, located in the rover's Ultra Clean Zone (UCZ). In the RLS system, the sample reference surface ($Z = 0$ position) is ideally on the top of the sample surface. The sample plane is defined as the average value of the sample reference surface considering the final sample distribution (roughness) after flattening within the RC. To ensure that the sample (and also the RLS CTs in the RC) is in the focusing range, the working distance between the RLS iOH mounting plane and the SPDS (ALD) sample plane surface position (also RLS CTs plane) must be 26 ± 0.2 mm.

During the nominal RLS operating scenario inside the ExoMars rover, the Raman iOH will focus[10] the laser light onto the sample (50 μm spot size) by moving its actuator mechanism (± 1 mm range), capable of displacing the iOH focusing optics (through z-axis) to an optimum location that allows effective excitation and collection of the signal during RLS operation with a positioning resolution of 5 μm. The Raman autofocus (AF) system uses the backscattered laser light to determine whether the iOH is focused on the optimal position (i.e., the acquisition position). The higher the intensity of the signal, the better the focus is considered to be. This focusing process is an important part of the scientific operations performed during the RLS acquisition sequence (fluorescence removal, integration time determination, and AF). The RLS algorithms are especially devoted to optimizing the SNR of the acquired spectra.[11,12]

The precise procedure for the RLS scan of a sample requires careful coordination with the SPDS.[1] The SPDS moves the sample RC in steps of 200–400 μm following a transect line underneath the RLS iOH. RLS assumes two main modes for sample scanning analysis: an automatic scan[13] of at least 20 points at fixed steps covering the entire powdered surface and a cooperative mode at precise positions with relevant interest for the mission objectives as determined by detailed inspection of the data produced by the MicrOmega instrument.[14]

The spectral analysis of crushed samples provides a number of scientific advantages over the analysis of bulk

samples, including the fact that the crushed/mixed material enables a deeper and more complete sample analysis, which could reveal interesting material characteristics that are not apparent at the surface of the bulk sample.[15,16] However, powdered sample analysis presents some additional challenges for the operation of the RLS instrument because the quality of the spectra obtained is highly dependent on the final sample morphology and the topography presented for analysis (e.g., grain size, distribution, and flatness). (1) Small grains could be damaged by the laser excitation source (if dark materials such as iron oxides, hydroxides, and/or carbonaceous matter are present), and the background signal is more significant in the acquired Raman spectra. In addition, if the typical grain size is small compared with the RLS spot diameter, there is the possibility that multiple grains will be illuminated and spectral bands associated with two or more mineral phases will be apparent in the spectra obtained. This leads to the less precise individual identification capability of the instrument. Larger grain sizes improve the Raman quality (as a consequence of the amount of material that is illuminated by the focusing cone) but induce difficulties for focusing the laser as discussed in more detail below. (2) The lower distribution gives a sample roughness profile, in which the AF is only necessary for fine optimization, and a larger distribution clearly implies the need of focusing at each point. The large fraction of grains increases the risk and complexity associated with AF mechanism work, which could be a potential risk for final Raman performances. (3) The flattening process could also introduce surface flatness issues: extra-large grains (e.g., >1 mm) could drag particles through the surface, creating variations in the surface profile.

Clearly, the sample preparation processes, resulting grain size distribution, and flattening process are critical aspects of the RLS instrument performance, and they are related to the instrument mineral identification capabilities and the overall scientific performance of the instrument. Once the capabilities and performance of the RLS Engineering and Qualification Model (EQM) have been demonstrated,[17] the biggest challenge for RLS is in dealing with these uncertainties. For that reason, the RLS EQM has been comprehensively tested to demonstrate that the ALD SPDS QM sample grain distribution and flattening processes are compatible with the RLS performance requirements. Two objectives are addressed in this paper. First (1) is the demonstration that the RLS EQM is capable of identifying key mineral phases under nominal operational scenarios and using representative samples that have been crushed by the SPDS Qualification Model (QM) in order to produce realistic grain size distributions. The mineral identification of the RLS EQM is then to be compared with data obtained with Raman laboratory equipment and the RLS ExoMars Simulator. The second aspect to be considered (2) is the distance uncertainty between the RLS iOH and the sample that arises from variations in the sample flatness in the final ALD QM configuration (i.e., with the RLS EQM fully assembled in the ALD) after sample preparation and processing performed with the SPDS QM.

2 | MATERIALS AND METHODS

To address the objectives covered in this article, a set of tests was performed on crushed samples produced by the SDPS QM system (following crushing processes fully representative of those that will be employed during surface operations) that provides grain size distributions similar to those produced by the Flight Model (FM) system. The samples were delivered to the ALD instrument team for analysis by the three analytical instruments. Various tests were programmed by the RLS team, ensuring operations were fully representative of those expected to be performed on the surface of Mars by the ExoMars rover and in a representative environmental scenario. The main objective of these tests is to confirm that the RLS instrument meets its scientific requirements given the grain size distributions produced by the SPDS. A comprehensive set of Raman analyses was also performed on the crushed samples using two additional Raman instruments in order to help fully assess the performance of the RLS. In summary, three different measurement campaigns were completed:

1. Tests performed with a *Laboratory Micro-Raman* at the University of Valladolid (UVa) to identify interesting material features in the provided samples. The lab equipment was operated manually by the user with a microscope (micromode) utilized to identify the different mineral distributions across the sample.
2. Tests performed with the *RLS ExoMars Simulator*,[18–20] also located at UVa, to analyze the provided samples in automatic scanning mode. This process simulates the nominal RLS operating mode. The identified material was then compared with the micromode results.
3. Tests performed with the *RLS EQM*[17] at INTA (Madrid) in a representative system testing framework that simulates all of the RLS interfaces (operational, power, data, and sample preparation) in order to confirm compatibility with the provided samples. The RLS EQM scanned the sample automatically according to the nominal RLS operating scenario. The materials identified by the RLS EQM were then

compared with the data obtained from the RLS ExoMars Simulator and the Raman laboratory equipment.

To achieve the second objective stated in this article and to complete the analytical study of the RLS sample processing chain, the final positioning of the sample with respect to the analytical instruments inside the ALD also has to be demonstrated. In particular, for RLS, the flatness process shall ensure that the sample plane will be positioned at the correct distance to the RLS IOH for operation.

4. Another test campaign was performed at TAS-I (Turin) with the ALD QM fully integrated (SPDS QM and RLS EQM) and the powder sample in the RC presented to the RLS EQM for scanning of the sample according to the nominal operation scenario. Specifically, the primary aims of this test were, first of all, to ensure the operation completion by analyzing powder samples in an end-to-end scenario and to obtain the final sample flatness by using the AF motor position feedback (motor position in every spot after AF algorithm execution) to determine how critical the AF function is in the RLS operation sequence.

2.1 | SPDS QM crushed samples

Sample crushing, with a grain size average of 250 μm, was performed with the ALD/SPDS CS QM controlled by a flight-like electronic unit and associated software. The CS is a miniaturized jaw crusher capable of crushing Martian sample cores with diameters up to 10 mm and lengths up to 35 mm. The material is crushed between a fixed and a moving metallic jaw, the latter actuated by an eccentric drive shaft. The crushing process can be modulated, rotating the jaws in order to compress or to loosen sample in the crushing volume. During ALD tests, the sample crushing process adopted was fully representative of that planned for surface operations. While milling, the samples fracture into smaller grains. Smaller particles fall through the jaws gap, which open up to 0.5 mm during the crushing cycle. The sample powder produced is collected in a dosing funnel and subsequently distributed to the analytical instruments.

Along the ALD testing campaign, from development to qualification, several samples were crushed, and the obtained powders were provided to instrument teams for analysis. A crushing test campaign with the CS QM was performed together with individual ALD instrument teams. The samples specifically selected to meet the objectives of this study are natural and may contain other minor phases, which have been already detected on Mars. They have particular relevance to astrobiological studies and were collected from Martian analog sites that in recent years have been extensively investigated by scientists directly involved in the development of the instrumentation aboard the rover.

Several samples were considered for the analysis with the analytical instruments (e.g., claystone with high calcium content). On average, the crushing produced more than 0.002 L of powdered material. The grain size distribution of the sample material depends on the specific nature of the material and on the gap between the jaws. After performance of a dedicated trade-off, the gap was tuned to meet the instrument's requirements to produce powder with an average grain size of 250 μm and with 90% of grains between 50 and 500 μm.

Three of the samples were evaluated by the three different RLS models for mineral identification (Objective 1) and one more sample to ensure operation completion after sample processing into the ALD (Objective 2).

1. *Gypsum from Sorbas* (southeast SPAIN) provided by the RLS PI. Gypsum is a calcium sulfate that has been detected on Mars by both orbiters[21] and rovers.[22] It is interesting from an astrobiological perspective because it can be formed in an environment that includes water (a fundamental element for the proliferation of life). Furthermore, studies of previous terrestrial analogs show that this mineral is capable of preserving biomarkers.[23] In this context, gypsum karst of Sorbas is one of the highlighted examples over the world for marine gypsum precipitation during the Messinian Salinity Crisis. Furthermore, the presence of caves also makes the Sorbas basin a suitable site for studying subsurface mechanisms of mineral precipitation, some of them mediated by microorganisms that could be Martian analogs.[24] Although the material was not shaped in the form of a cylindrical drill core, the pieces were smaller than 1 cm and could therefore be crushed straightforwardly. The crushed sample was split into two different containers for scientific investigation. Samples IDs: *Sample_01*: Gypsum (Portion_1) and *Sample_02*: Gypsum (Portion_2).

2. Mix of same proportion of two different materials: *jarosite* provided by RLS and *kaolinite* by MicrOmega scientists. Previous studies have shown that jarosite on Mars has been found in association with kaolinite phyllosilicate.[25] It is thought that these mineral associations may be due to weathering within paleo-ice deposits.[26] Consequently, the mixture provides a relevant test for assessing the capability of the RLS instrument to identify the composition of samples containing heterogeneous mineralogy. In this case,

the crushed fragments were deposited in a dedicated container. Sample ID: *Sample_03*: Jarosite_and_Kaolinite.

3. According to Objective 2, one additional sample was tested with the RLS EQM to verify the sample roughness level after sample preparation process completion (flatness) in the ALD QM. Organic free samples of porous fused silica (FS-120) were crushed for testing during the full ALD qualification test campaign (in a Mars-like environment). *Sample_04* (ALD sample).

2.2 | Laboratory micro-Raman equipment test description

The micro-Raman laboratory instrument was used to analyze the coarse grains produced by the ALD/SPDS QM in detail, with Raman spectra acquired from individual grains. The laboratory equipment is composed of a 633 nm excitation laser signal; the spectrometer, which was assembled in the laboratory with commercial components, is composed of a Research Electro-Optics LSRP-3501 laser (helium–neon), a Kaiser Optical Systems, Inc. (KOSI), a Holographic Filtered Probe Head (HFPH) Raman probe, a KOSI Holospec1.8i spectrometer, and an Andor DV420A-OE-130 CCD. The system is coupled to a Nikon Eclipse E600 microscope that can focus the excitation source onto the sample with several different interchangeable, long-working-distance objectives (i.e., 5, 10, 20, 50, and 100). Raman spectra were collected in the wavenumber offset range 130–3780 cm^{-1}, with a mean spectral resolution of 4 cm^{-1}. Data acquisition was performed using the Hologram 4.0 software.

Three samples were evaluated during this test (Sample_01, Sample_02, and Sample_03) at UVa. The sample material was deposited and flattened into the aluminum support compartments (one for each compound). Sufficient powder was placed into the compartments to ensure it filled the entire cubicle (Figure S1), and then the compartment was placed below the micro-Raman head for the analysis.

To better disclose the mineralogical heterogeneities of the samples, the spots of interest were visually selected by the operator, who made use of the microscope coupled to the Raman spectrometer to focus the excitation on mineral grains presenting different appearances in terms of both color and opacity. Inhomogeneities at the microscopic level were noted in every sample. Samples were manually scanned with the microscope, spot by spot, looking for interesting features, where impurities or organic biomarkers were present (i.e., interesting grains). Once the sample fraction is observed with the microscope, the particular point is placed below the optical head for Raman acquisition. Before acquisition of the Raman spectra, the laser excitation source was focused on the powder sample, and the acquisition parameters (integration time and number of accumulations) were optimized to maximize the SNR of the spectra.

2.3 | RLS ExoMars simulator test description

The RLS ExoMars Simulator[27] provides a tool to analyze and evaluate the capabilities of the instrument in an ALD-like scenario. The system emulates the ExoMars rover SPDS by means of a system that simulates the flattening and positioning of the powder sample (see Figure S2), allowing the automation of a complete Raman measurement cycle. The basic RLS simulator configuration developed in UVa provides a laser excitation source of 532 nm with an irradiance at the sample of 0.45 kW/cm^2 in a spot of 50 μm diameter. The irradiance selected for the RLS instrument is a compromise between system lifetime, performance (in terms of Raman band SNR), and the possibility of sample damage. The RLS SPDS simulator consists of an XYZ micrometric positioning system with an optical head attached to the *z*-axis and an RC attached to the XY positioners.

The RLS simulator was programmed in an automatic mode by varying the arrangement of the points to be measured and synchronizing the sample scanning with the nominal Raman operation sequence. The number of spots analyzed was set to 10, with 100 μm steps between each spot. With this program, there is a very slight overlap of points, so a precise and complete mapping of the sample is achieved. The spectral acquisition is automatically performed for each of the focused points along the line of transect. The number of accumulations was set to 10, and the integration time was automatically calculated to achieve 90% of the CCD Full-Well Capacity (FWC)[19] to optimize the SNR of the final spectrum at each point. By definition, in RLS, the signal level average is measured as the 5-point intensity average of the Raman signal at ± 30 cm^{-1} from the maximum band position, and the standard deviation of the noise distribution is measured in the difference spectrum of two consecutive spectral measurements in the spectral range covering 100 cm^{-1} at both sides of the mentioned main band starting at ± 30 cm^{-1}.

The three materials (Sample_01, Sample_02, and Sample_03) analyzed were deposited individually into an RC with the same design characteristics as those used for surface operations. The sample was positioned for scanning and analysis under the simulator optical head after the representative flattening process had been performed (Figure S2).

2.4 | RLS EQM system test framework description

The RLS EQM model is the previously manufactured and tested model representative of the "real" flight instrument.[17] It provides a wavelength-stabilized 532 nm laser, with a narrow bandwidth, thermally controlled for optimum performance. The RLS EQM irradiance is close to 1.8 kW/cm^2 on sample, with a 50 μm diameter spot. The CCD detector can be thermally cooled to reduce dark signal noise.[17,28]

The RLS EQM was used to analyze representative crushed samples in a representative system testing framework in the laboratory.[28] The system testing framework enables instrument control with a set of dedicated system scripts or telecommands that are provided via the RLS rover vehicle simulator (RVIS), which was specifically developed to simulate the rover power, data, and communications interfaces to the RLS. The RLS Instrument Data Analysis Tool (IDAT)[29] was specially developed for the RLS instrument and was used for RLS data interpretation (including both spectral and engineering information).

To reproduce the complete RLS operation scenario on Mars, the RLS EQM units (ICEU, SPU, and iOH) were installed according to the real ALD configuration with the RLS iOH facing the samples (Figure S3). A Sample Holder System was used to position the SPDS QM crushed samples. The system was also able to emulate the ALD SPDS sample movements for both x-axis and y-axis displacements. With the AF mechanism placed at the "Home" position (position: 0 mm—in the middle of the range), the sample system holder plane (Z) was placed such that the acquisition position achieved in every sample could be adjusted by using the RLS iOH focus mechanism (±1 mm).

RLS RVIS scripts were programmed in different ways by varying the arrangement of some system and configuration parameters to handle the (1) RLS EQM and the (2) Sample Holder System operation so that a sequence could be created to simulate the ALD and RLS operation on ground.

To ensure the correct RLS EQM operation, the RLS instrument needs to be properly configured. The instrument configuration allowed the activation of the scientific algorithm (integration time calculation and AF) during the operation sequence execution and the activation of the thermal control mask for instrument performance optimization: set the correct laser temperature (24.8°C) to guarantee that the excitation wavelength is well controlled at 532 nm and control the CCD temperature to improve the instrument SNR[30] when considered. The number of accumulations was also set to 10 CCD images. The RLS instrument was commanded

considering the RLS nominal operation scenario. The RLS operative sequence starts with the acquisition of several dark frames for baseline correction. Then, the RLS thermal control is activated, to ensure all RLS elements are with the correct temperature. Before any Raman acquisition, the iOH AF function has to be executed. The AF procedure provides a specific iOH motor position (focus position) at every scanned spot, which is nominally placed on the sample surface. After AF execution in every spot, the final position of the iOH motor is calculated by the system by reading backscattered telemetry (TM) of the AF photodiode current placed in the Raman Laser Assembly (RLA) of the RLS instrument. When the signal is maximized, the laser is at optimum focus, and the iOH focus is sent to the calculated position. The motor achieves this final position with a precision of 5 μm. Then, the Automatic Raman acquisition is performed after execution of the RLS scientific algorithms, when the integration time is optimized in every spot, achieving the 80% of the CCD full-well capacity. The Sample Holder System movements were synchronized with the instrument operative sequence by moving the motor y-axis in steps of 100 μm, and the commanded number of spots was set to five per sample. This process allowed analysis of a large area of the sample by the RLS EQM.

2.5 | RLS EQM in the ALD QM flight-like scenario

The ALD QM is a platform model which allows for the execution of the end-to-end tests in a Mars environment and the verification of the complete sequence of operations defined for the sample processing chain. It will be integrated into the ExoMars rover Ground Testing Model (GTM), which is dedicated for operation validation on the ground, building representative sequences with the ALD PPLs and samples involved. To conclude with the ALD qualification campaign, a set of end-to-end tests was planned with the ALD and the instruments to confirm that the sample preparation and distribution processes in a flight-like scenario are compatible with the analytical instrument under real conditions (Figure S4). The ALD RVIS supports ALD QM experiments and functional tests at TAS-I by simulating the rover vehicle-dedicated interfaces of the various PPLs and the overall ALD in terms of power, data, and SPDS sample processing and preparation operations.

Rover RC position tolerance has to be inside the RLS focusing range after the SPDS flattening process. As the sample flatness distributed into the RC changes at every flattening process, the RLS AF was able to reach the

sample surface in all the operational conditions along the complete sample scanning. During sample scanning, the RLS EQM can check that the sample is well positioned under the RLS iOH by utilizing the AF function. This validation can be performed by determining in every spot the best focus position, accounting for the uncertainty introduced by the sample flattening process. Nominally, the best focus position is in the sample surface, so by targeting a sufficient number of spots during the sample scanning process, the sample surface profile or sample roughness can be obtained.

Responding to this need, a dedicated procedure was defined to command the ALD QM and RLS EQM during the sampling scans. The RLS EQM was configured and programmed with the same parameters that were used during the system tests at INTA (i.e., scientific algorithms, thermal control activation, and number of accumulations). The number of spots to be analyzed was typically 20 (depending on the timing constraints for using the ALD) with synchronization of the sample movements with the RLS operation: performing the AF and Raman acquisition operations sequentially at every achieved spot. And to complete the operational scenario, the ALD/SPDS QM was programmed to scan a large sample area. On the external side of the sample, the SDPS was moved in steps of 400 μm, and in the middle of the sample, it was moved in 100 μm steps.

The compatibility of the AF function and the complete RLS EQM Raman performance in the nominal final scenario will be presented. Motor position results can be compared with those obtained during the RLS integration process where the RLS CTs were aligned by shimming the RLS iOH, placing it in the correct working distance with respect to the CT sample plane.

3 | RESULTS AND DISCUSSION

3.1 | Crushed sample performance study results with RLS instruments

The three different RLS models were tested using representative crushed samples, to provide an evaluation of instrument performance as a function of operational scenario.

3.1.1 | Micro-Raman laboratory equipment: Results obtained in manual mode

Several grain fractions were analyzed in each and every sample, with individual grain sizes in the range 30–150 μm. Sample_01, Sample_02, and Sample_03 were evaluated under this test configuration. As expected, Raman analysis in manual mode after visual microscopic observation allows for easy and clear identification of minor or trace compounds within the powdered samples.

Main materials presented in the samples were gypsum as displayed in Figure 1; the characteristic vibrational modes of calcium sulfate were clearly detected at
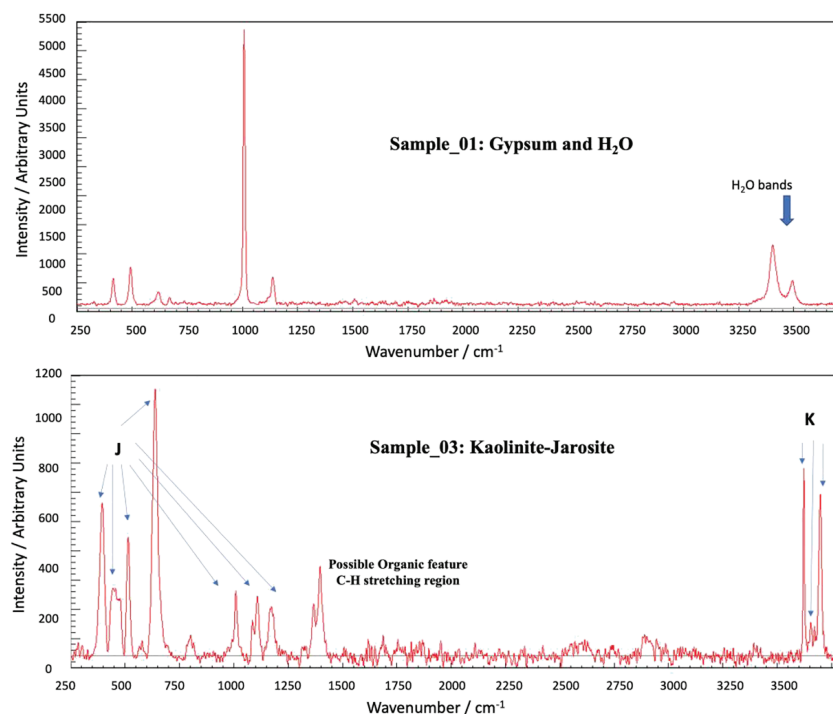

FIGURE 1 Micro-Raman lab. Equipment Raman spectra: Sample_01_Gypsum and Sample_03 Jarosite_and_Kaolinite

416, 495, 623, 674, 1008, and 1143 cm^{-1} in both Sample_01 and Sample_02. In addition to these, the stretching vibrational modes of water molecules were also identified at 3402 and 3492 cm^{-1}, respectively, confirming the hydration of the detected mineral phase. Also, kaolinite and jarosite in Sample_03 Jarosite_and_Kaolinite material were clearly detected with the micro-Raman (Figure 1). On one hand, the main peaks of jarosite were detected at 352, 433, 624, 1006, 1100, and 1152 cm^{-1}. On the other hand, the characteristic OH vibrational modes of kaolinite were found at 3622,

3651, 3672, and 3693 cm^{-1}, although its main peak at 131 cm^{-1} cannot be observed due to the edge filter implemented in the system.

Apart from the main expected materials, the system was also able to detect some interesting secondary components in the material, a sample of which is presented below (see Figure 2). Sample_01 exhibits the presence of goethite (Raman shift 299, 387, and 550 cm^{-1}, together with the main peak of gypsum at 1008 cm^{-1}) together with additional minor/trace phases. Most of the Raman spectra collected from this sample displayed a high
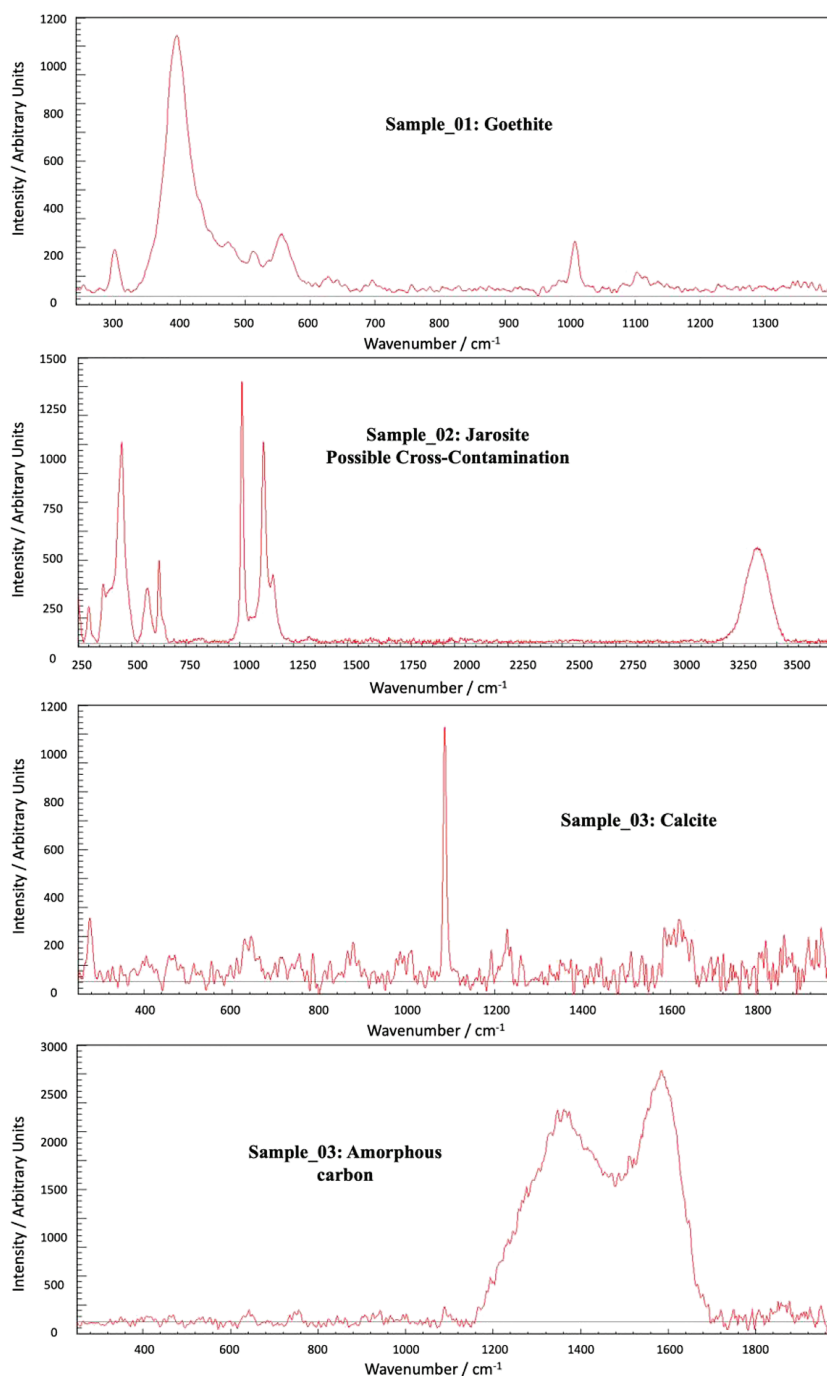

FIGURE 2 Sample_01: goethite with gypsum. Sample_02: jarosite (possible cross-contamination). Sample_03: calcite and amorphous carbon (possible cross-contamination)

fluorescence background. As explained elsewhere,[31] fluorescence emission from geological samples could be generated by multiple sources, including the presence of biogenic organics. However, further studies are needed to clearly disclose the origin of this emission. In Sample_02, traces of jarosite (Sample_03) were observed in the gypsum sample. It is suspected that this could have arisen as a consequence of a cross-contamination issue (from a previous crushing process of the SDPS QM). Several materials were identified in Sample_03 such as calcite (Raman shift 281 and 1085 cm^{-1}) and amorphous carbon (double band around 1370 and 1590 cm^{-1}). As presented in the work of Pasteris and Wopenka,[32] the Raman detection of disordered carbonaceous material within a geological matrix could be related to the presence of degraded organic matter. However, complementary analysis needs to be performed to establish its organic/inorganic origin.

The positive results obtained with the micro-Raman instrument when using the microscope in manual mode are use as reference to compare the equipment detection and operation capabilities with regard to other Raman instruments: RLS ExoMars simulator and RLS EQM. Table S1 summarizes the minerals detected with micro-Raman mode in the evaluated samples.

3.1.2 | RLS ExoMars simulator: Result obtained in automatic mode

The three separate samples were evaluated with the RLS ExoMars simulator for results comparison: Sample_01, Sample_02, and Sample_03. The automatic mode is a blind test that ensures the RLS ExoMars simulator can cover the complete sample during the scanning, where a specific point for material analysis cannot be selected. Considering this constraint and as was observed during

the micro-Raman analysis, the three major materials were detected in all of the samples.

The admixture dejamming in Sample_03 exhibited quite noisy spectra. Although the kaolinite signal was very clear, the jarosite signal was very weak, making it very difficult to detect in the spectra even with baseline correction (Figure 3). In this regard, it must be underlined that the different wavelengths of the excitation sources employed by micro-Raman (633 nm) and RLS (532 nm) instruments strongly affect the detection of jarosite. Indeed, green wavelengths are more absorbed by red minerals (as jarosite) than red excitation lasers wavelengths. For this reason, when similar acquisition parameters (time of exposition and number of accumulations) are used, the Raman signals of jarosite detected by the RLS tend to be weaker than those observed by micro-Raman.

Additionally, gypsum and carotenoids[33,34] from algae (Raman shift 1158 and 1518 cm^{-1}) were detected in Sample_01 and Sample_02 (Figure 4). The positive detection of a carotenoid with the simulator (compared with the lack of signature observed with the micro-Raman system) is due to the fact that a greater number of points were measured on the sample and that the wavelength of the RLS/simulator (532 nm) is more suitable for the detection of these types of compounds than the 633 nm excitation signal used in the micro-Raman system. H$_2$O bands were also present in both samples, although they were not evident in all spots analyzed along the transect scans. The spectral quality was reasonably good, and the carotene biomarker can be readily identified. These results are consistent with visual observation and the Raman data obtained from the micro-Raman measurements with just one single spot acquisition, which reinforces the importance of having enough points for sample observation. Intensity differences in the gypsum water bands indicate orientation of the grains in the
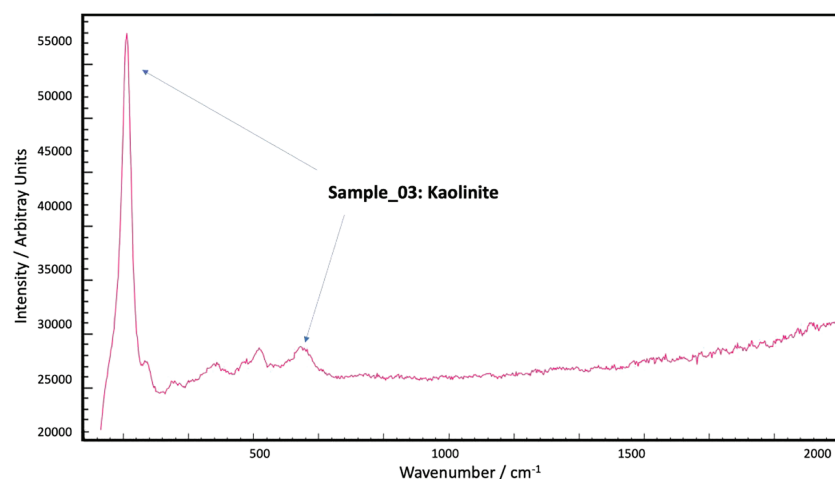

FIGURE 3 Raman Laser Spectrometer ExoMars simulator spectra from Sample_03. Kaolinite after baseline correction
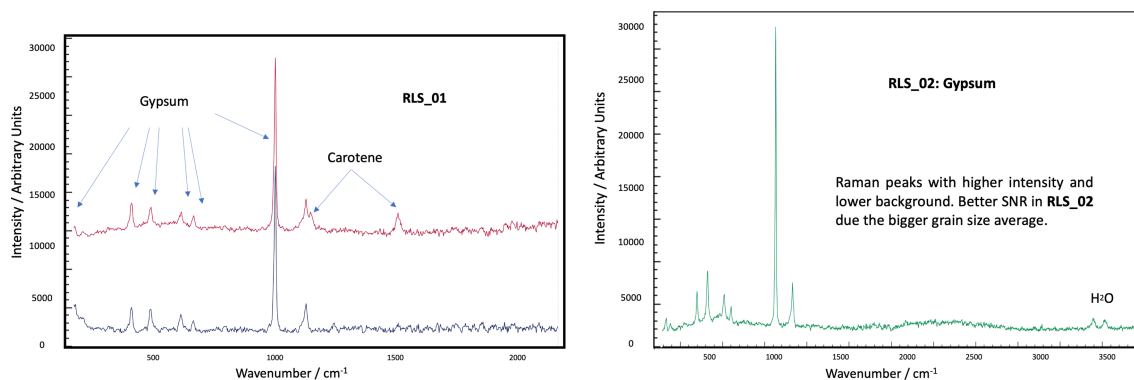
FIGURE 4   Raman Laser Spectrometer (RLS) ExoMars simulator spectra. Sample_01: gypsum and carotene. Sample_02: gypsum and H_2O bands. SNR, signal-to-noise ratio
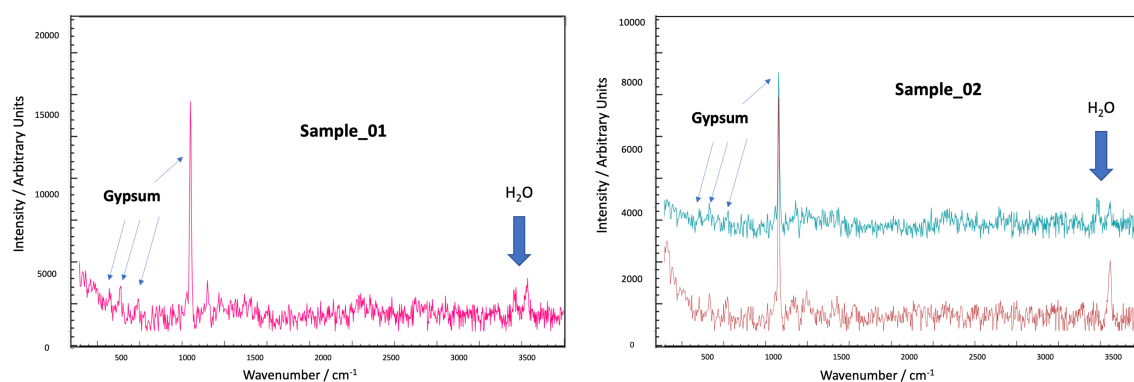

FIGURE 5   Raman Laser Spectrometer Engineering and Qualification Model spectra. Sample_01: gypsum. Sample_02: gypsum. Both images show H_2O bands and baseline correction

sample, that is, usually because they have an appreciable different grain size. The quality of the obtained Raman spectra was very good, and H_2O was easily identified, although no carotenoids were observed.

Some traces of potential biosignatures were evident in the gypsum sample material (i.e., carotene in Sample_01). The automatic mode allowed identification of the biogenic compound. Sample_01 and Sample_02 exhibited differences mainly in the general spectral background and in the SNR, caused in principle by the different grain size of the analyzed material, which is bigger at Sample_02. No additional material was observed during the automated scan, including no evidence for the cross-contamination detected with the micro-Raman equipment scan.

3.1.3 | RLS EQM: Results obtained in automatic mode

The three crushed samples, Sample_01, Sample_02, and Sample_03, were evaluated with the RLS EQM in

an automatic scan mode under the system test framework configuration at INTA. The obtained results are very similar to those obtained with the RLS ExoMars simulator.

Gypsum was clearly identified in both Sample_01 and Sample_02. Sample_02 presented a larger background signal when studied with the RLS EQM. The vibrational modes of OH were clearly detected in both samples, confirming the hydration of the mineral phase. However, as highlighted in the red spectra provided in Figure 5, some of the targeted spots only displayed the second OH peak around 2490 cm^{-1}. As many factors could lead to this unusual spectroscopic observation, further studies need to be performed to explain this detection.

In order to investigate the effects of temperature on the performance of the RLS EQM (i.e., from room temperature to relevant Martian conditions), the thermal control of the CCD detector was activated. Dark signal noise in the RLS EQM detector was reduced by commanding the CCD to a colder temperature ($-10°C$). As a result, the SNR is considerably improved.[30]
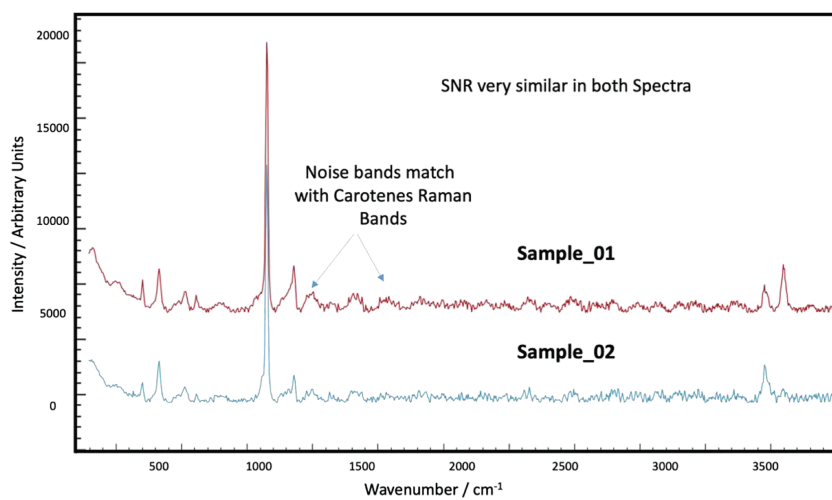
FIGURE 6 Raman Laser Spectrometer Engineering and Qualification Model spectra at −10°C. Comparison of Sample_01 gypsum and possible carotenoids and Sample_02 gypsum with baseline correction. SNR, signal-to-noise ratio
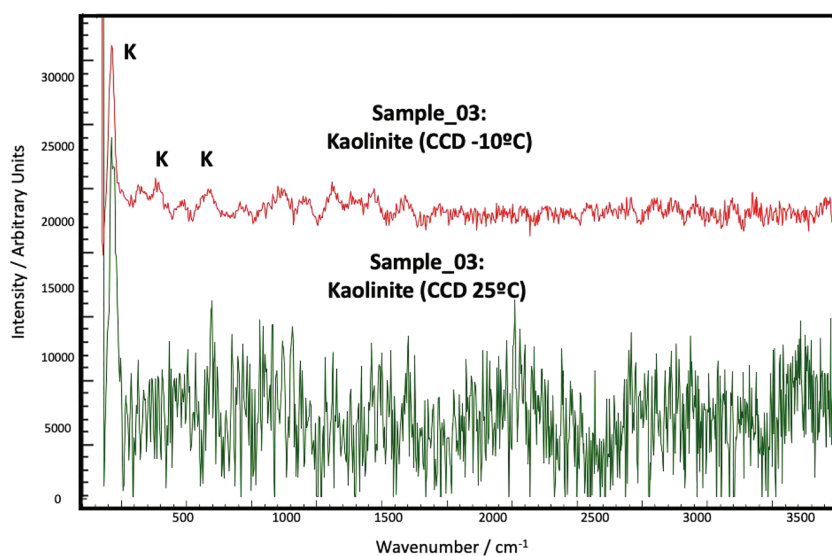

FIGURE 7 Raman Laser Spectrometer Engineering and Qualification Model spectra at −10°C versus 25°C. Sample_03: Jarosite_and_Kaolinite sample. Baseline-corrected spectra

Comparison of the spectra obtained for Sample_01 and Sample_02 showed that the SNR is very similar after baseline removal (Figure 6). Organic compounds (carotenoids) are very hard to see, even with noise reduction. The position of these small bands with very low SNR matches with the position of the main carotene peaks; however, some extra work needs to be performed with the data to discriminate the low signal Raman from the noise signal.

Kaolinite is clearly observed in Sample_03 (Figure 7), but jarosite is hard to identify at ambient temperature due to increased system noise. Again, the activation of the CCD thermal control commanded to −10°C improves the spectral quality and SNR and makes easier some extra kaolinite Raman peaks. But even with very low noise levels and baseline correction,

the jarosite was very difficult to see as happened also with the RLS simulator. As only five spots were analyzed with the RLS EQM (the RLS operational scenario considers at least 20 spots), the statistical probability of detecting more interest features on the sample could be maximized when more points along the sample will be analyzed.

3.2 | Sample flatness results with RLS EQM in the ALD QM flight-like scenario

The last step was to ensure the compatibility of the ExoMars ALD sample preparation process (crushing, dosing, and flattening) with RLS instrument acquisitions,

FIGURE 8 Sample roughness obtained after sample scanning with the iOH motor position. ALD, Analytical Laboratory Drawer; AF, autofocus; iOH, internal optical head; PSHS, powdered sample handling system; RLS, Raman Laser Spectrometer
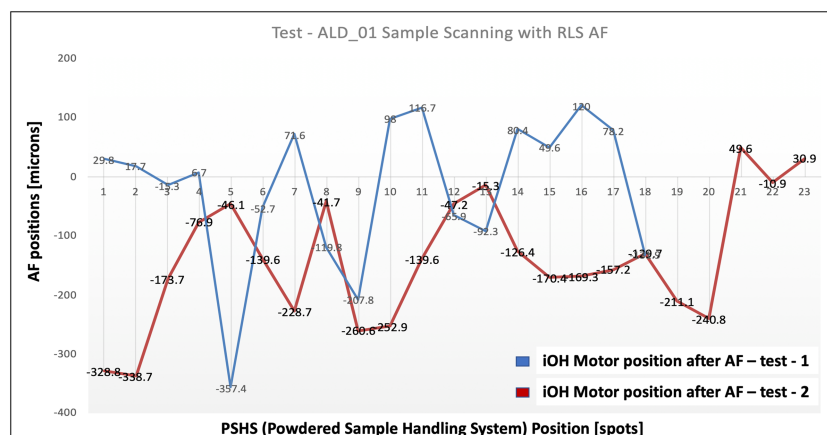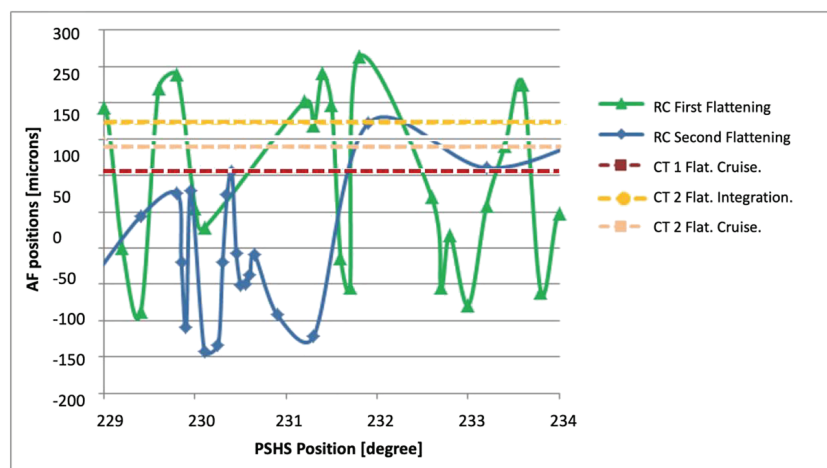

FIGURE 9 RLS EQM AF scan over RLS EQM CTs (cruise and integration environments). RLS EQM AF scan over Sample_04 after two flattening processes: green first scan, and blue second scan. AF, autofocus; CT, calibration targets; EQM, Engineering and Qualification Model; RC, refillable container; RLS, Raman Laser Spectrometer

checking that the sample plane in the RC (following the flattening process) is placed at the correct distance from the RLS iOH EQM.

The RLS EQM was commanded according to the nominal operation sequence over the sample by using the AF function to absorb the sample surface uncertainty in order to reach the best focus position in all the analyzed spots. By scanning the complete sample with the RLS AF system (several spots), the final sample roughness and sample plane can be obtained with the iOH motor position reached at every spot after AF execution, demonstrating the sample is well positioned and distributed. Several tests were performed with the RLS EQM on Sample_04 in automatic mode, according to the nominal operation scenario.

Preliminary results obtained with the RLS AF telemetry during the sample scanning show that the sample plane in the RC was at the correct working distance. The average of the sample flattening positions obtained with the RLS AF system is −106 μm with a deviation between grains of 130 μm (see Figure 8). Results obtained with the RLS AF match with the SPDS/QM information received from mechanism testing and flatness measurements, where the average sample plane was fixed at −0.2 mm. This information can be used for AF algorithm optimization.

In another test execution, the RLS EQM CTs and the powder sample were scanned to be able to compare the sample plane position with respect to the RLS CT sample plane position (CT_1 and CT_2). The green plot corresponds to the RLS AF scanning positions along the RC surface after a first flattening process; the blue plot corresponds to the RC surface after a second flattening process. The sample surface of the two RLS CTs is reported at different pressure environmental conditions (see Figure 9). In the worst-case scenario, the distances from the sample surface plane and CT surface planes are within a range of 250 μm, much lower than the AF mechanism range that is ±1 mm.

TABLE 1 Summary of minerals detected by RLS on samples evaluated under different test condition

ID	Sample name	Laboratory (micro-Raman) Material detected	Op. mode	RLS simulator Material detected	Op. mode	RLS EQM Material detected	Op. mode
Sample_01	Gypsum from Sorbas (Spain). Portion_1	- Gypsum (including its characteristic H_2O absorption bands) - Goethite	Manually scanning the sample spot by spot	- Gypsum (including its characteristic H_2O absorption bands) - Carotene	Automatically scanning 10 spots analyzed	- Gypsum (including its characteristic H_2O absorption bands)	Automatically scanning five spots analyzed at ambient and Mars environment CCD
Sample_02	Gypsum from Sorbas (Spain). Portion_2	- Gypsum (including its characteristic H_2O absorption bands) - Goethite - Jarosite (possible cross-contamination)		- Gypsum (including its characteristic H_2O absorption bands)		- Gypsum (including its characteristic H_2O absorption bands)	($-10°C$)
Sample_03	Jarosite and kaolinite	- Kaolinite and jarosite - Goethite - Calcite - Amorphous carbon		- Kaolinite		- Kaolinite	

Abbreviations: EQM, Engineering and Qualification Model; RLS, Raman Laser Spectrometer.

4 | CONCLUSIONS

The analyses performed with the micro-Raman Laboratory Equipment, the RLS ExoMars simulator, and the RLS EQM demonstrate that the RLS instrument can acquire good-quality spectra from crushed and flattened samples, such as those provided by the SPDS QM. The test results show that the RLS instrument can obtain very positive results when also using the microscope for visual mineral identification. The micro-Raman instrument is a powerful tool for the identification of minor or trace compounds in powdered samples. The implementation of the microscope (or camera) combined with the Raman spectroscopy is identified as a clear improvement for the development of new instrumentation for future exobiology exploration. Furthermore, these joint tests have also shown that the RLS ExoMars simulator and RLS EQM obtain very good results when operating in automatic mode (i.e., without human intervention or other instruments). One conclusion that deserves particular attention is that the best option for the operational sequence is to maximize the number of points instead of spending a long time acquiring one spectrum at a particular spot. Another goal that was achieved was the investigation of how spectral quality varies with temperature for both the RLS EQM and the ExoMars simulator (i.e., during the transition from room temperature to relevant Martian conditions). In this case, it was clearly demonstrated that spectral quality improves very significantly as temperature is reduced for the RLS EQM. This is due to the reduction in detector dark signal because the device used is a non-inverted CCD. In order to evaluate the tests performed under the different environment conditions where the SPDS QM crushed samples were evaluated by RLS, Table 1 compares the main results obtained by every RLS model under those conditions: The operational mode and identified materials are also presented.

Finally, the sample presentation process performed by the SPDS QM (end-to-end scenario with the ALD QM fully integrated) allowed the completion and determination of overall operational performance. This means that the RC and RLS CT sample planes are reachable by the RLS AF mechanism in all circumstances, so the nominal operational sequence could be completed according to expectation (calibration over the CT and sample scan over the RC). Results obtained allowed unambiguous identification of several different minerals present in the sample according to the grain size distribution and flattening process, stressing the importance of using the RLS AF algorithm in the final operational context of the mission. The final sample preparation uncertainty can clearly be absorbed (i.e., accounted for) using the iOH focus mechanism with a range of ±1 mm. The AF

algorithm can be optimized by setting the motor default position at the sample plane value obtained after the sample scan.

Future work will focus on the improvement of the definition of the RLS nominal operational sequence for RLS on Mars. Several tests are programmed with the RLS ExoMars simulator at UVa, the RLS FS at INTA, and the Rover GTM (RLS EQM) at TAS-I, mimicking the RLS sample measurement cycle. A trade-off between the number of acquisition spots and the operational resources on Mars (power, data, and timing) needs to be performed for science optimization.

ACKNOWLEDGMENTS

ORCID

Carlos Perez Canora https://orcid.org/0000-0002-9575-1258

Andoni Moral https://orcid.org/0000-0002-6190-8560

Jesus Zafra https://orcid.org/0000-0001-6041-7172

Marco Veneranda https://orcid.org/0000-0002-7185-2791

Gonzalo Ramos https://orcid.org/0000-0001-7831-1050

Guillermo Lopez-Reyes https://orcid.org/0000-0003-1005-1760

REFERENCES

[1] J. L. Vago, F. Westall, Pasteur Instrument Teams, S. Landing, A. J. Coates, R. Jaumann, O. Korablev, V. Ciarletti, I. Mitrofanov, J.-L. Josset, M. C. De Sanctis, J.-P. Bibring, F. Rull, F. Goesmann, H. Steininger, W. Goetz, W. Brinckerhoff, C. Szopa, F. Raulin, F. Westall, H. G. M. Edwards, L. G. Whyte, A. G. Fairén, J.-P. Bibring, J. Bridges, E. Hauber, G. G. Ori, S. Werner, D. Loizeau, R. O. Kuzmin, R. M. E. Williams, J. Flahaut, F. Forget, J. L. Vago, D. Rodionov, O. Korablev, H. Svedhem, E. Sefton-Nash, G. Kminek, L. Lorenzoni, L. Joudrier, V. Mikhailov, A. Zashchirinskiy, S. Alexashkin, F. Calantropio, A. Merlo, P. Poulakis, O. Witasse, O. Bayle, S. Bayón, U. Meierhenrich, J. Carter, J. M. García-Ruiz, P. Baglioni, A. Haldemann, A. J. Ball, A. Debus, R. Lindner, F. Haessig, D. Monteiro, R. Trautner, C. Voland, P. Rebeyre, D. Goulty, F. Didot, S. Durrant, E. Zekri, D. Koschny, A. Toni, G. Visentin, M. Zwick, M. van Winnendael, M. Azkarate, C. Carreau, the ExoMars Project Team, *Astrobiology* **2017**, *17*, 471.

[2] F. Rull, S. Maurice, I. Hutchinson, A. Moral, C. Perez, C. Diaz, M. Colombo, T. Belenguer, G. Lopez-Reyes, A. Sansano, O. Forni, Y. Parot, N. Striebig, S. Woodward, C. Howe, N. Tarcea, P. Rodriguez, L. Seoane, A. Santiago, J. A. Rodriguez-Prieto, J. Medina, P. Gallego, R. Canchal, P. Santamaría, G. Ramos, J. L.

[3] J. P. Bibring, V. Hamm, C. Pilorget, J. L. Vago, MicrOmega Team, *Astrobiology* **2017**, *17*, 621.

[4] C. Pilorget, J. P. Bibring, *Planet. Space Sci.* **2013**, *76*, 42.

[5] G. Fred, B. W. Brinckerhoff, R. François, G. Walter, D. R. Danell, S. A. Getty, S. Sandra, M. Helge, S. Harald, R. D. Arevalo Jr., B. Arnaud, F. Caroline, G. Andrej, U. J. Meierhenrich, V. T. Pinnick, S. Fabien, S. Cyril, J. L. Vago, L. Robert, M. D. Schulte, B. J. Robert, D. P. Glavin, G. Noel, L. Xiang, F. H. W. van Amerom, the MOMA Science Team, *Astrobiology* **2017**, *17*, 655.

[6] P. Ribes-Pleguezuelo, A. M. Inza, M. G. Basset, P. Rodríguez, G. Rodríguez, M. Laudisio, M. Galan, M. Hornaff, E. Beckert, R. Eberhardt, A. Tünnermann, *Optim. Eng.* **2016**, *55*, 116107.

[7] J. F. Cabrero, M. Fernández, M. Colombo, D. Escribano, P. Gallego, R. Canchal, T. Belenguer, J. García, J. M. Encinas, L. Bastide, I. Hutchinson, A. Moral, C. P. Canora, J. A. R. Prieto, C. Gordillo, A. Santiago, A. Berrocal, F. Rull, in International Conference on Space Optics, **2018**, 347.

[8] G. Ramos, M. Sanz-Palomino, A. G. Moral, C. P. Canora, T. Belenguer, R. Canchal, J. A. R. Prieto, A. Santiago, C. Gordillo, D. Escribano, G. Lopez-Reyes, F. Rull, in Proc. SPIE Optical Engineering + Applications Conference, **2017**, 10377.

[9] G. Lopez-Reyes, A.G. Moral, F. Rull, J.A. Rodriguez, C. Pilorget, J.P. Bibring, J.L. Vago, in GeoRaman Conference, **2018**, 3.

[10] G. Ramos, M. Sánz Palomino, A. G. Moral, C. Pérez, T. Belenguer, R. Canchal, J. A. R. Prieto, A. Santiago, C. Gordillo, D. Escribano, G. López Reyes, F. Rull, *J. Raman Spectrosc.* **2020**, *51*, 1761. https://doi.org/10.1002/jrs.5765

[11] G. Lopez-Reyes, F. Rull, *J. Raman Spectrosc.* **2017**, *48*, 1654.

[12] G. Lopez-Reyes, Development of Algorithms and Methodological Analyses for the Definition of the Operation Mode of the Raman Laser Spectrometer Instrument, PhD Thesis, Universidad de Valladolid (Spain) **2015**, 266. https://uvadoc.uva.es/handle/10324/17717

[13] C.P. Canora, A.G. Moral, F. Rull, G. Ramos, L. Seoane, J.A.R. Prieto, J. Zafra, C. Quintana, S. Ibarmia, J. Saiz, G. López-Reyes, T. Belenguer, R. Canchal, P. Rodriguez, P. Santamaria, A. Berrocal, M. Colombo, P. Gallego, A. Santiago, C. Gordillo, D. Escribano, M. Sanz-Palomino, J. Cabrero, in 16th Asia Oceania Geosciences Society Meeting, **2019**, Singapore (Republic of Singapore), PS03-A011.

[14] G. Lopez-Reyes, C. Pilorget, A. G. Moral, J. A. Manrique Martinez, A. Sanz, A. Berrocal, M. Veneranda, F. Rull, J. Medina, V. Hamm, J. P. Bibring, J. A. Rodriguez, C. P. Canora, E. Mateo-Marti, O. Prieto-Ballesteros, E. Lalla, J. L. Vago, *J. Raman Spectrosc.* **2020**, *51*, 1. https://doi.org/10.1002/jrs.5832

[15] G. Lopez-Reyes, F. Rull, G. Venegas, F. Westall, F. Foucher, N. Bost, A. Sanz-Arranz, A. Catala-Espi, A. Vegas, I. Hermosilla-Rodriguez, A. Sansano, J. Medina, *Eur. J. Mineral.* **2013**, *25*, 721.

[16] F. Foucher, G. Lopez-Reyes, N. Bost, F. Rull-Perez, P. Rüßmann, F. Westall, *J. Raman Spectrosc.* **2013**, *44*, 916. https://doi.org/10.1002/jrs.4307

[19] Vago, *Astrobiology* **2016**, *17*, 627. https://doi.org/10.1089/ast.2016.1567

[17] A. G. Moral, F. Rull, S. Maurice, I. B. Hutchinson, C. P. Canora, L. Seoane, G. Lopez-Reyes, J. A. R. Prieto, P. Rodriguez, G. Ramos, Y. Parot, O. Forni, *J. Raman Spectrosc.* **2019**, *51*, 1771. https://doi.org/10.1002/jrs.5711

[18] G. Lopez-Reyes, F. Rull, G. Venegas, F. Westall, F. Foucher, N. Bost, A. Sanz, A. Catalá-Espí, A. Vegas, I. Hermosilla, A. Sansano, J. Medina, *Eur. J. Mineral.* **2013**, *25*, 721. https://doi.org/10.1127/0935-1221/2013/0025-2317

[19] G. Lopez-Reyes, F. Rull Pérez, *J. Raman Spectrosc.* **2017**, *48*, 1654. https://doi.org/10.1002/jrs.5185

[20] G. Lopez-Reyes, A. Perez Oliveros, A. Sanz, F. Rull, in *GeoRaman Conference*, **2012**, Nancy (France), 111.

[21] C. M. Weitz, J. L. Bishop, J. A. Grant, *Planet. Space Sci.* **2013**, *87*, 130. https://doi.org/10.1016/j.pss.2013.08.007

[22] M. Nachon, S. M. Clegg, N. Mangold, S. Schröder, L. C. Kah, G. Dromart, A. Ollila, J. R. Johnson, D. Z. Oehler, J. C. Bridges, S. Le Mouélic, O. Forni, R. C. Wiens, R. B. Anderson, D. L. Blaney, J. F. Bell III, B. Clark, A. Cousin, M. D. Dyar, B. Ehlmann, C. Fabre, O. Gasnault, J. Grotzinger, J. Lasue, E. Lewin, R. Léveillé, S. McLennan, S. Maurice, P.-Y. Meslin, W. Rapin, M. Rice, S. W. Squyres, K. Stack, D. Y. Sumner, D. Vaniman, D. Wellington, *J. Geophys. Res. Planets* **2014**, *119*, 1991. https://doi.org/10.1002/2013JE004588

[23] K. Counter Benison, F. J. Karmanocky III, *Geology* **2014**, *42*, 615. https://doi.org/10.1130/G35542.1

[24] F. Rull, G. Venegas, F. Gázquez, J. M. Calaforra, J. Martínez-Frías, A. Sansano, J. Medina, in *2nd Analog Sites for Mars Missions Conference*, **2013**, Washington (USA), 4012.

[25] J. Cuadros, C. Mavris, J. R. Michalski, J. M. Nieto, J. L. Bishop, S. Fiore, *Icarus* **2019**, *330*, 30. https://doi.org/10.1016/j.icarus.2019.04.027

[26] J. R. Michalski, P. B. Niles, in *42nd Lunar and Planetary Conference*, **2011**, The Woodlands (Texas), 1926.

[27] G. Lopez-Reyes, M. Veneranda, A. González Martín, J. A. Manrique, A. Moral, C. Perez-Canora, J. A. Rodriguez Prieto, A. Sanz Arranz, J. Saiz, E. Lalla, M. Konstantinidis, O. Prieto Ballesteros, J. Medina, L. M. Nieto Calzada, F. Rull, *J Raman Spectrosc* **2021**, *1*. https://doi.org/10.1002/jrs.628114

[28] J. Zafra, J. Saiz, L. Seoane, C. Quintana, S. Ibarmia, J.A.R. Prieto, C.P. Canora, A.G. Moral, G. Lopez-Reyes, F. Rull, in *Simulation and EGSE for Space Programmes – sesp2019 conference*, **2019**, Noordwijk (The Netherlands), 1.

[29] G. Lopez-Reyes, J. Saiz, A. Guzmán, A. Moral, C. Pérez, F. Rull, J.A. Manrique, J. Medina, the RLS team, in *European Planetary Science Congress*, **2018**, Berlin (Germany), 1132.

[30] C.P. Canora, A.G. Moral, F. Rull, S. Maurice, I. Hutchinson, G. Ramos, G. López-Reyes, T. Belenguer, R. Canchal, J.A.R. Prieto, P. Rodriguez, P. Santamaria A. Berrocal, M. Colombo, P. Gallago, L. Seoane, C. Quintana, S. Ibarmia, J. Zafra, J. Saiz, A. Santiago, A. Marin, C. Gordillo, D. Escribano, M. Sanz-Palomino, in *European Planetary Science Congress*, **2017**, Berlin (Germany), 1002.

[31] F. Košek, A. Culka, A. Rousaki, P. Vandenabeele, J. Jehlička, *J. Raman Spectrosc* **2020**, *51*, 1636. https://doi.org/10.1002/jrs.5667

[32] J. D. Pasteris, B. Wopenka, *Astrobiology* **2003**, *3*, 727. https://doi.org/10.1089/153110703322736051

[33] H. Horiue, M. Sasaki, Y. Yoshikawa, M. Toyofuku, S. Shigeto, *Sci. Rep.* **2020**, *10*, 7704.

[34] J. Jehlička, H. G. M. Edwards, K. Osterrothová, J. Novotná, L. Nedbalová, J. Kopecký, I. Němec, A. Oren, *Philos Trans. A Math. Phys. Eng. Sci.* **2014**, *199*, 372. https://doi.org/10.1098/rsta.2014.0199

SUPPORTING INFORMATION

Additional supporting information may be found in the online version of the article at the publisher's website.